

Mid-Infrared Gas Sensor Based on Mutually Injection Locked Quantum Cascade Lasers

Adonis Bogris, Andreas Herdt, Dimitris Syvridis, and Wolfgang Elsässer, *Senior Member, IEEE*

Abstract—We present experimental investigations of a novel mid-infrared gas sensor relying on a laser system consisting of two quantum cascade sources mutually coupled with each other. The free-space path between the two lasers contains the sensing cell which is filled with the gas of interest. This laser system proves to be a very interesting dynamical system which can offer enhanced detectivity when compared to a conventional direct absorption spectrometer utilizing a laser, the gas cell, and a detector. We present comprehensive investigations of the operation regimes under which the laser system behaves as an efficient sensor and demonstrate its dependence on critical parameters such as the coupling strength between the two lasers and their bias currents. The experimental study is supported by numerical simulations, which provide a theoretical understanding of the underlying mechanisms. A six fold improvement of the sensitivity in a N_2O absorption spectroscopy experiment is demonstrated in comparison to a conventional direct absorption spectrometer. This sensitivity improvement is exhibited for a wide range of N_2O concentrations.

Index Terms—semiconductor lasers, optical injection, infrared spectroscopy, Gas detectors.

I. INTRODUCTION

LASER spectrometers based on quantum and interband cascade lasers (QCLs and ICLs) operating in the mid-infrared (MIR) provide an exciting prospect for trace gas sensing as they enable access to the fingerprint region where many molecules of both fundamental and applied interest have strong absorption cross-sections and high spectral selectivity [1]–[3]. Many different spectroscopic techniques have been realized in the past in order to improve the detectivity of gas sensors, most of them exploiting the enhancement by cavities trapping the light which effectively increase the path length through the absorption cell by several orders of magnitude [4]–[9]. Although cavity enhancement such as Cavity Ring-Down Spectroscopy

(CRDS) [10] or optical-feedback cavity-enhanced absorption spectroscopy (OF-CEAS) [11] are boosting the sensing performance, they also introduce complexity, increase the size and pose stability issues which make these gas sensors less practical in real life applications. For this reason, the simple scheme of a laser targeting a typical MIR detector after passing through a multi-pass cell is preferred instead in practical scenarios. In this paper, we propose and experimentally analyze a sensing scheme of this type which improves the sensitivity of the typical mid-infrared gas sensing system with marginally higher complexity than that of typical absorption spectrometers. The scheme relies on the mutual coupling between two quantum cascade lasers. In this scheme, the absorption cell is placed within the path of mutual injection. One of the two lasers, or both of them could be ramped in current in order to scan the absorption line. The light propagation through the absorption line affects the optical injection into both lasers and disturbs the laser system as a whole. Taking into account that the laser system is a dynamical system tending to operate stably, the change of the optical power in the optical coupling path is a perturbation which non-linearly affects the system and influences the stability operating point [12]. This change is reflected in the power of both lasers and can be utilized for sensitive spectroscopic measurements. The comparison of this scheme with a typical spectrometer consisting of a laser, the absorption cell and the detector proves that the proposed system offers a six times enhancement compared to the conventional direct absorption spectrometer. In order to provide an explanation of the experimentally obtained results we numerically simulated the laser system relying on the modified rate equation model tailored for mutually coupled QCLs. The results of the theoretical and experimental analysis coincide very well showing in fact that the sensitivity enhancement takes place at the boundary of the locking bandwidth characterized by a sharp transition from the non-locking to locking state, especially when the lasers are operated close to its threshold.

The paper is structured as follows. First we describe the experimental setup and measurement methods in Section II. The rate equation simulation model utilized for the theoretical analysis of the laser system is presented in Section III. The experimental results and the numerical results supporting the findings are presented in Section IV. Section V contains the basic conclusions of our work.

II. EXPERIMENTAL SETUP

For the mutual locking experiments a commercially available ALPES Distributed Feedback (DFB) QCL and a Fabry Perot (FP) laser provided by III-V Lab were used. The ALPES QCL

Manuscript received June 1, 2016; revised August 3, 2016; accepted August 23, 2016. Date of publication August 26, 2016; date of current version October 18, 2016. This work was supported in part by the European Communities Seventh Frame-work Programme FP7/2007-2013 under Grant 288304 (STREP CLARITY) and in part by the COST Action MP1204 “TERA-MIR radiation: materials, generation, detection and applications.”

A. Bogris is with the Department of Informatics, Technological Educational Institute of Athens, Athens 12243, Greece and also with the Department of Informatics and Telecommunications, National and Kapodistrian University of Athens, Athens 15784, Greece (e-mail: abogris@teiath.gr).

A. Herdt and W. Elsässer are with the Institute of Applied Physics, Technische Universität Darmstadt, Darmstadt 64289, Germany (e-mail: andreas.herdt@physik.tu-darmstadt.de; elsasser@physik.tu-darmstadt.de).

D. Syvridis is with the Optical Communications Laboratory, Department of Informatics and Telecommunications, National and Kapodistrian University of Athens, Athens GR-15784, Greece (e-mail: dsyvridi@di.uoa.gr).

Color versions of one or more of the figures in this paper are available online at <http://ieeexplore.ieee.org>

Digital Object Identifier 10.1109/JSTQE.2016.2603341

emits at 2194.5 cm^{-1} and its tuning range is 2 cm^{-1} . The maximum output power is 30 mW at $-10 \text{ }^\circ\text{C}$. The FP laser emits at 2230 cm^{-1} and its output power does not exceed 5 mW . The temperature of this laser was set to $25 \text{ }^\circ\text{C}$. Although the two lasers have an intrinsic wavenumber difference of approximately 30 cm^{-1} , they manage to lock to each other by properly tuning the FP laser current as will be shown in Section IV. The FP laser is driven by a homemade battery source which offers better stability compared to commercially available current sources. The light emitted by the DFB laser passes through an absorption cell filled with N_2O . Beam splitters are utilized in order to guide the optical emissions from one laser to the other and from the lasers to a low noise liquid nitrogen cooled mercury cadmium telluride (MCT) detector with a detection bandwidth of 50 MHz . The AC signal of the detector that corresponds to the DFB laser intensity but also to the intensity of the coupled laser system is sent to an oscilloscope for time-trace analysis. The variation of the optical injection is accomplished with the use of a variable neutral density filter (NDF) placed in the path between the two sources. A Fourier Transform Infrared Spectrometer (FTIR) with a maximal resolution of 0.075 cm^{-1} is utilized in order to perform optical spectrum measurements that will be presented in Section IV.

III. SIMULATION MODEL

The band structure of the considered QCL is described with a 3 level approximation [13], [14]. The laser emission occurs at the transition from level 3 to level 2, while the transition from level 2 to level 1 is accompanied with an optical-phonon emission. The radiative and non-radiative transitions from level 3 to levels 2 and 1 are also taken into account. The carrier and field dynamics in the 3-level QCL approximation are described by rate equations (RE) for the carrier number population for each level and the electrical field of the mutually coupled lasers. Hence, the RE system takes into account the mutual injection effect which is not present in unidirectional models [12]–[14]. The modified RE system assuming single mode operation reads:

$$\frac{dN_{3m,s}}{dt} = \frac{\eta_{m,s} I_{m,s}}{q} - \frac{N_{3m,s}}{\tau_{32m,s}} - \frac{N_{3m,s}}{\tau_{31m,s}} - g_{m,s}(N_{3m,s} - N_{2m,s})S_{m,s} + F_{3m,s} \quad (1a)$$

$$\frac{dN_{2m,s}}{dt} = \frac{N_{3m,s}}{\tau_{32m,s}} - \frac{N_{2m,s}}{\tau_{21m,s}} + g_{m,s}(N_{3m,s} - N_{2m,s})S_{m,s} + F_{2m,s} \quad (1b)$$

$$\begin{aligned} \frac{dE_{m,s}}{dt} = & \frac{1}{2} \left[Z_{m,s} g_{m,s} (N_{3m,s} - N_{2m,s}) - \frac{1}{\tau_{ph,m,s}} \right] \\ & \times (1 + i\alpha_{m,s}) E_{m,s} + E_{sp,m,s} + \frac{\sqrt{\kappa_{inj,m,s}}}{\tau_{r,m,s}} \\ & \times E_{s,m}(t - T) e^{i\omega T} \mp i\delta\omega E_{m,s} \end{aligned} \quad (2)$$

In (1), the indices m,s correspond to master and slave lasers. Master-slave configuration represents the case of unidirectional coupling, when one of the two lasers is externally injected into the other one without being affected by its radiation by using an

TABLE I
PHYSICAL AND STRUCTURAL PARAMETERS USED IN THE CALCULATIONS

Parameter	Value
Laser length, L	2 mm
Number of stages, Z	25
Photon lifetime, τ_p	4.3 ps
Current injection efficiency, η	0.15
Gain coefficient, g	$0.6 \times 10^4 \text{ s}^{-1}$
Linewidth enhancement factor, α	2
Refractive index	3.2
Emission wavelength, λ	$5 \text{ } \mu\text{m}$
Phonon scattering time $3 \rightarrow 2$, τ_{32}	2.13 ps
Phonon scattering time $3 \rightarrow 1$, τ_{31}	2.1 ps
Phonon scattering time $2 \rightarrow 1$, τ_{21}	0.5 ps

optical isolator [12], [15]. Although this is not the case in the bidirectional coupling, we keep this terminology considering that the master laser is the DFB laser with a wavenumber being closely linked to the absorption cell and which will be operated above threshold in all studied operating regimes. The same laser is also more suitable to be used in the comparison case of a conventional spectrometer relying on continuous wave (CW) operating QCLs. The FP laser is less practical for spectroscopy applications due to its multi-wavelength emission. With a proper adjustment of the operating conditions, it can be driven to single-mode operation forced by the external injection of the DFB laser mode once it coincides with a cavity mode of the slave laser [15].

In (1), $N_i = N_i(t)$ is the carrier number at the corresponding energy level, $S = S(t)$ is the photon number and equals to $S = |E|^2$ where E is the complex electrical field described in (2), g is the gain coefficient, q is the electron charge and Z the number of stages. Moreover, τ_{ph} is the photon lifetime, τ_{ij} the transition characteristic times, I is the injection current and η is the injection efficiency. The terms $F_i = F_i(t)$ ($i = 1, 2, 3, S$) represent the noise contribution which follows the Langevin force formulation. More details regarding the noise part of the model and its numerical and theoretical treatment are provided in [13]–[15]. In (2), as already reported, E represents the electrical field for both master and slave lasers, α is the linewidth enhancement factor and T is the optical delay corresponding to the path distance between the two lasers. The term $\omega = (\omega_m + \omega_s)/2$ corresponds to the mean value of the radial frequency of the free running master and slave lasers, whilst the term $\delta\omega = (\omega_m - \omega_s)/2$ is the half of their frequency detuning. E_{sp} corresponds to the spontaneous noise emission term and is a complex number [13], κ_{inj} is the external injection ratio corresponding to the portion of the optical electrical field externally coupled to each laser and τ_r is the round-trip time of the laser cavity. The basic laser parameters are provided in Table I. Although, in a real system the two lasers will exhibit significant dissimilarities in internal parameters, we have considered identical parameters for both lasers without loss of generality. What is important in this paper is to study the behavior of the system at different operating points of the two lasers and as a function of κ_{inj} , $\delta\omega$. The integration of (1), (2) has been performed using a modified first order method for ordinary differential equations. In order to ensure the model convergence, the integration step used in the simulations was $dt = 0.1 \text{ ps}$.

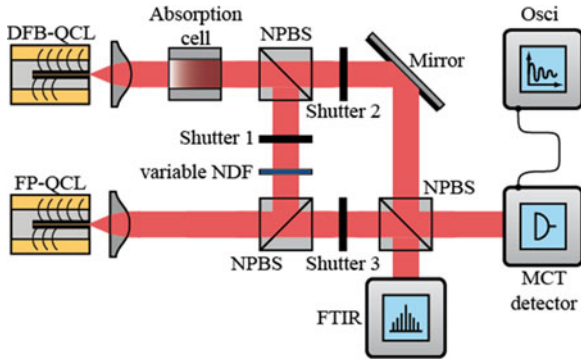


Fig. 1. Experimental setup. The absorption cell can be filled with a sample gas and its pressure and concentration can be varied. The optical alignment allows us to either measure the optical power behind the absorption cell or determine the spectra with the FTIR.

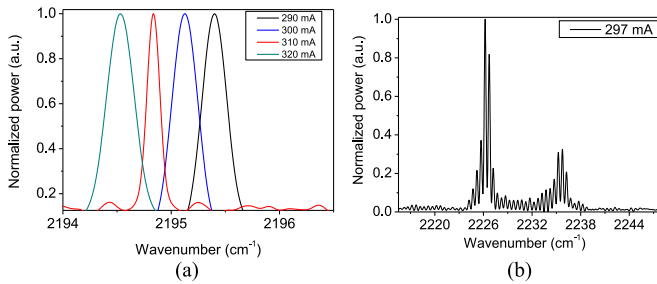


Fig. 2. Optical spectrum of the free running DFB (a) and FP (b) lasers.

IV. RESULTS AND DISCUSSION

A. Basic Properties of Mutually Coupled QCLs—Experiments

Our first goal was to experimentally identify the regimes under which the laser system would be driven to single-mode operation. The CW operation reveals that the laser system is a locked system exhibiting the highest possible optical power at one lasing mode. In this experiment the variable attenuator and the sensing cell depicted in Fig. 1 were removed. The DFB laser was operated at -15°C and the FP lasers at 25°C . Before showing the FP laser emitted spectrum under mutual coupling, for the sake of completeness we also present the DFB and FP laser spectra when operated as free running lasers. The results are shown in Fig. 2 and clearly indicate the single-mode operation of the DFB laser and the dependence of the lasing mode on the bias current. The multi-mode operation of the FP and the intrinsic wavenumber detuning of approximately 30 cm^{-1} can be also observed.

In the mutual coupling experiment, the current of the FP was manually varied and its optical spectrum was recorded with the use of the FTIR as depicted in Fig. 3. The DFB laser current was set to 334 mA corresponding to a wavenumber of 2193 cm^{-1} . Under specific bias conditions, the slave laser is forced to emit on the DFB laser mode (blue line and red line) despite their intrinsic wavenumber detuning of 30 cm^{-1} . A similar behavior was theoretically and experimentally verified for QCLs in [15] for unidirectional coupling and is attributed to the tendency of a

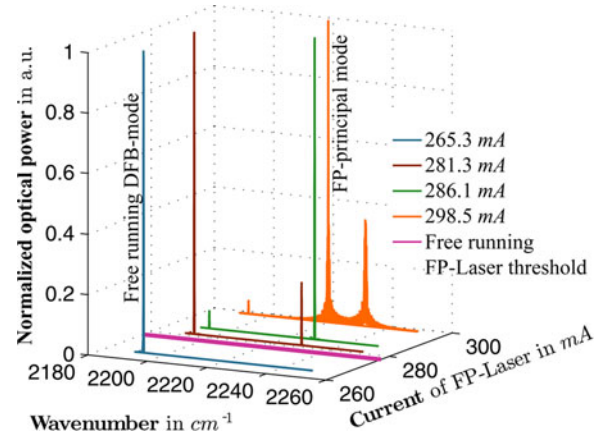


Fig. 3. Optical spectrum of the FP laser under mutual locking for different bias current values. It is evident that for bias currents close to threshold, the FP laser is injection locked by the DFB laser mode emitting at the same wavenumber.

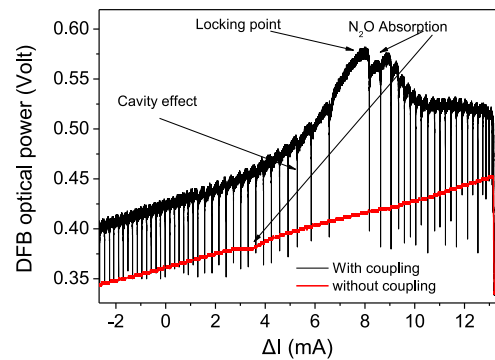


Fig. 4. DFB laser optical power as a function of DFB laser relative current ($I_{\text{DFB,AVG}} = 301.5\text{ mA}$) with (black) and without (red) mutual coupling with the FP laser (Experiment).

laser to oscillate at the frequency of an externally injected light provided that this frequency is in the vicinity of a cavity mode of the slave laser. In the same figure there exist many interesting regimes where pure locking, no locking and the generation of new tones at more distant wavelengths are observed.

The present work focuses on the sensing properties of the scheme. From this viewpoint, it is important to note that FP is efficiently locked to DFB laser emission when operated close to threshold (Fig. 3). Furthermore, as a sensor, the device needs to scan a range of wavenumbers and detect the absorption peaks representing the spectral signature of molecules of interest. As a first step, we scanned the wavenumber of the DFB laser and identified its power response under mutual coupling with the FP laser. Fig. 4 shows the experimentally recorded master power at the MCT detector. The DFB laser was biased with 301.5 mA at -10°C and its current was swept at 137 Hz with an amplitude of 20 mA . The FP was biased with 263.8 mA at 25°C (slightly below threshold). In this measurement the absorption cell is present and filled with 31 ppm of N_2O using air as buffer gas at a pressure of 280 hPa . For the sake of completeness, the power of the free running DFB laser is also included in the figure (red line). The impact of mutual coupling is evident; first, the master

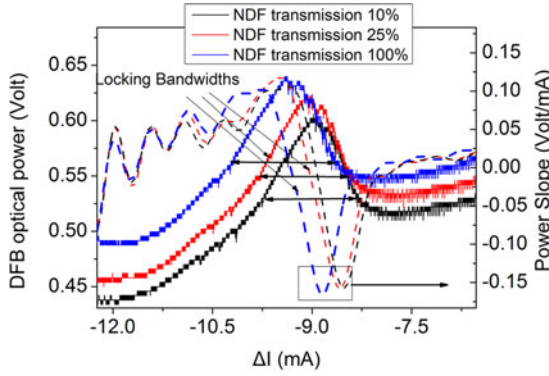


Fig. 5. DFB laser optical power and its slope as a function of the DFB laser relative current for three injection levels in the vicinity of injection locking.

power is globally increased as expected due to its interplay with the slave laser. Second, the power exhibits a local maximum which corresponds to the point where the optimal condition of injection locking has been achieved. Finally, the power is characterized by strong dropouts attributed to the combined influence of external cavity effect (similarly to what is observed in OF-CEAS systems) and the mode competition taking place in both lasers simultaneously. The latter effect may explain the non-periodic occurrence of the power swinging in opposition to what is observed for a laser subjected to optical feedback. The asymmetric profile of the optical power is attributed to the injection locking properties for non-zero linewidth enhancement factor of the lasers. Depending on the sign and the value of the linewidth enhancement factor of the slave laser, the latter does not exhibit a symmetric locking bandwidth with respect to its free running frequency. Although the QCLs are characterized by low α values (< 3), they also exhibit the asymmetric locking with respect to frequency detuning when operated above threshold as shown in [15]. This behavior has been observed for typical semiconductor lasers as well [21]. From the injection locking point of view, as already shown in [13], [15], the two lasers can be locked to each other within a specific frequency window, the so-called locking bandwidth which reflects the potential of a laser to oscillate in a cavity mode provided that proper amount of optical power is externally injected. Injection locking is extremely sensitive to injection strength especially when one of the two lasers is oscillating near threshold. One interesting feature is that the injection strength also affects the locking bandwidth; therefore a variation of the injection strength at the boundaries of the locking bandwidth would substantially affect the emission of the injection-locked laser. Most interestingly, this effect is taking place in a bidirectional way due to mutual injection which means that an enhancement of the power variations of both lasers similar to that offered by relevant cavity effects is expected. This behavior was experimentally verified with the use of the variable NDF. In Fig. 5, the master power is depicted for three different injection levels realized by the variable attenuator transmission. In this experiment, the absorption cell is not present. The bias currents for the two lasers are set to 301.5 mA for the DFB laser and 270 mA for the FP laser (close to threshold). The power was also properly filtered so as to remove the

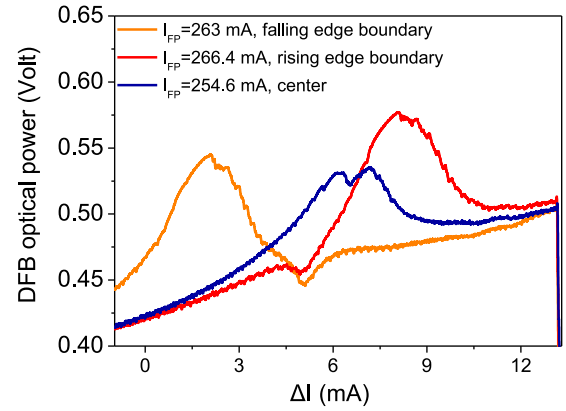


Fig. 6. DFB power for three different FP bias currents. The sensing cell contains 31 ppm of N_2O at 280 hPa. The falling edge boundary is the one that corresponds to the abrupt transition between the two states.

external cavity effects. The absolute power and its profile is substantially affected by the injection level showing higher power and a wider locking bandwidth at higher injection (blue line). Moreover, it is interesting to note that the power slope in terms of position and magnitude, especially that of the falling edge, is also highly dependent on the injection level (dashed curves). In order to verify this observation, we conceived experiments with the presence of the sensing cell filled with 31 ppm of N_2O at 280 hPa. By varying the FP-laser current in the neighborhood of the threshold value we succeeded in moving the absorption dip across the locking bandwidth. In Fig. 6, three time snapshots of the DFB laser intensity variations are depicted with the absorption dip being located at the center ($I_{FP} = 254.6$ mA) of the locking bandwidth and at the two boundaries ($I_{FP} = 263$ mA, $I_{FP} = 266.4$ mA). It is evident that the absorption dip is magnified at the falling edge of the locking bandwidth ($I_{FP} = 263$ mA) due to the higher slope and its higher dependence on the injection strength which is also affected by the presence of the absorbing gas. Therefore, the absorbing gas itself is not only affecting the power of the DFB laser but also the injection strength whose value mostly influences the locking boundary with the steeper response from locking to non-locking state.

B. Basic Properties of Mutually Coupled QCLs—Simulations

The indication of the unique properties of locking boundaries was first provided by the numerical simulations based on (1)–(2). Before conducting the experiments, we simulated the behavior of the system as a function of the injection strength κ_{inj} and the bias currents of the two lasers and we obtained similar results. The $\delta f = \delta\omega/2\pi$ parameter was varied from -4 GHz to 4 GHz and this variation is equivalent to applying a ramp signal in the current of one of the two lasers. As in the experiment, we recorded the steady state point of the master and slave powers. The behavior of the laser system was investigated in three operating regimes; slave below threshold, slave close to threshold, slave far above threshold. The threshold current amounts to 445 mA. In Fig. 7 we observe the dependence of both slave and master power slopes on κ_{inj} values, especially at the boundary of the sharp transition to injection locking

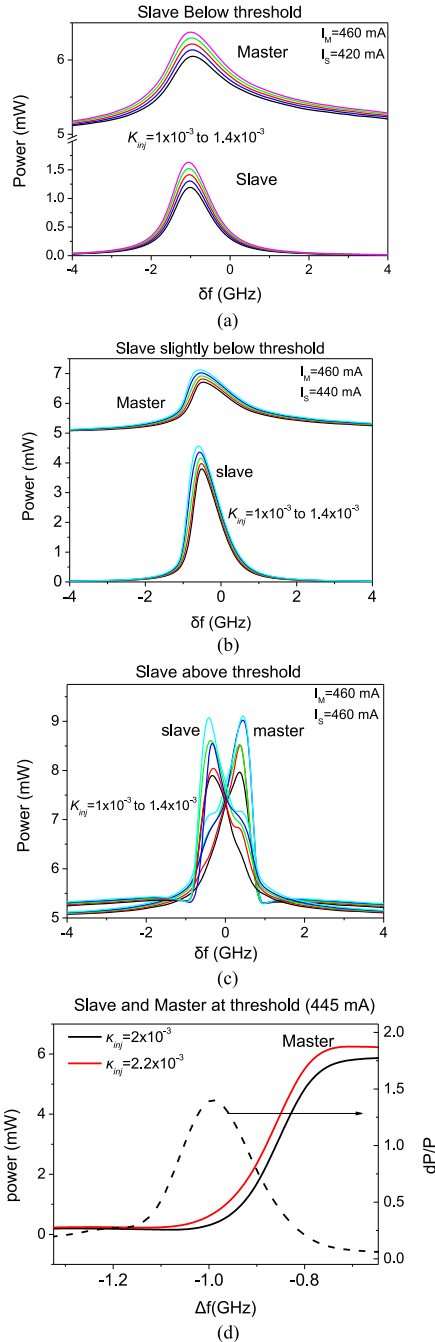


Fig. 7. The power of master and slave as a function of their detuning for different κ_{ij} values ranging from 1×10^{-3} to 1.4×10^{-3} in steps of 10^{-4} . The slave laser is operated below (a), around (b) and above (c) the threshold. (d) The power of master and the parameter dP/P when both lasers operate at threshold.

observed for the negative detuning due to the selected α parameter in the simulations. It is interesting to note that the slope change becomes more evident when the slave is operated at threshold and above. Far below threshold, the slave is reacting as a resonant device, therefore its response is symmetric with respect to δf [15]. As the current of the slave approaches the threshold, its response becomes asymmetric due to its non-zero α parameter. This asymmetry enhances the steepness of master transition from the non-locking to the locking-state

(Fig. 7(b)) which benefits the sensing process. In the experiments we verified this behavior and found empirically that the best operating regime under the sensing point of view for the operation of slave (FP laser in our case) is in the vicinity of the threshold of the FP laser. Above the threshold, the system becomes extremely nonlinear (Fig. 7(c)) and it is not easy to utilize it for sensing purposes. Apart from the increased nonlinearity, in the specific case of our experiment, the operation of the FP far above threshold does not ease its locking from the DFB laser injection as shown in Fig. 3. Our numerical analysis revealed that the enhancement provided by the locked system could be in the order of fifteen. This is shown in Fig. 7(d), where the normalized power difference dP/P between two master outputs for two injection levels having a 10% difference is estimated and depicted with a maximum value of 150%. This enhancement was obtained when both lasers were operated around threshold where the mutual injection has its major effect on the excitability of the laser system. This enhancement can not be exploitable due to noise and large instabilities manifesting in the vicinity of threshold. As it will be shown in the next paragraph, in a real system the enhancement is limited to lower values.

C. Sensing Performance

After having interpreted and discussed the qualitative properties of the laser system, in this paragraph we will present its sensing performance in comparison to what is offered by the typical absorption spectrometer consisting of the DFB laser, the sensing cell and the MCT-detector. For the spectroscopic measurements depicted in Fig. 8, the DFB laser was biased with 301.5 mA at -10°C and its current was swept at 137 Hz with an amplitude of 20 mA. The FP was biased at an injection current of 252.7 mA at 25°C . At this temperature, the slave was operated 10 mA below threshold. Fig. 8(a) shows the output power of the DFB laser emission as a function of DFB laser current with the current ramped with and without injection from the FP laser. We carefully adjusted the FP current properly to match the frequency of the absorption dip into the locking boundary of higher steepness. We calculated the ratio normalized derivative of the power $(dV/dI)/V$, because it is linearly connected to the absorption strength through the Beer-Lambert law. Thus we could provide a direct comparison of the improvement in absorption detectivity with and without injection. Fig. 8(a) shows clearly that the enhancement factor reflecting the comparison of the $(dV/dI)/V$ of the proposed spectrometer over the corresponding value of the conventional spectrometer is close to six. Fig. 8(b) shows the absorption coefficient of 31 ppm of N_2O at a pressure of 280 hPa which was determined using the conventional direct absorption spectrometer after performing Voigt fit in the curve of the signal voltage acquired at the MCT (Fig. 8(b)-top, grey line). Knowing the critical parameters of pressure, length of absorption cell, frequency of absorption line and temperature, we calculated the absolute concentration by using the Lambert-Beer law and HITRAN database.

We studied the proposed QCL-spectrometer at different points of the locking bandwidth via the chosen value of the FP-QCL current and the results are depicted in Fig. 9. In this

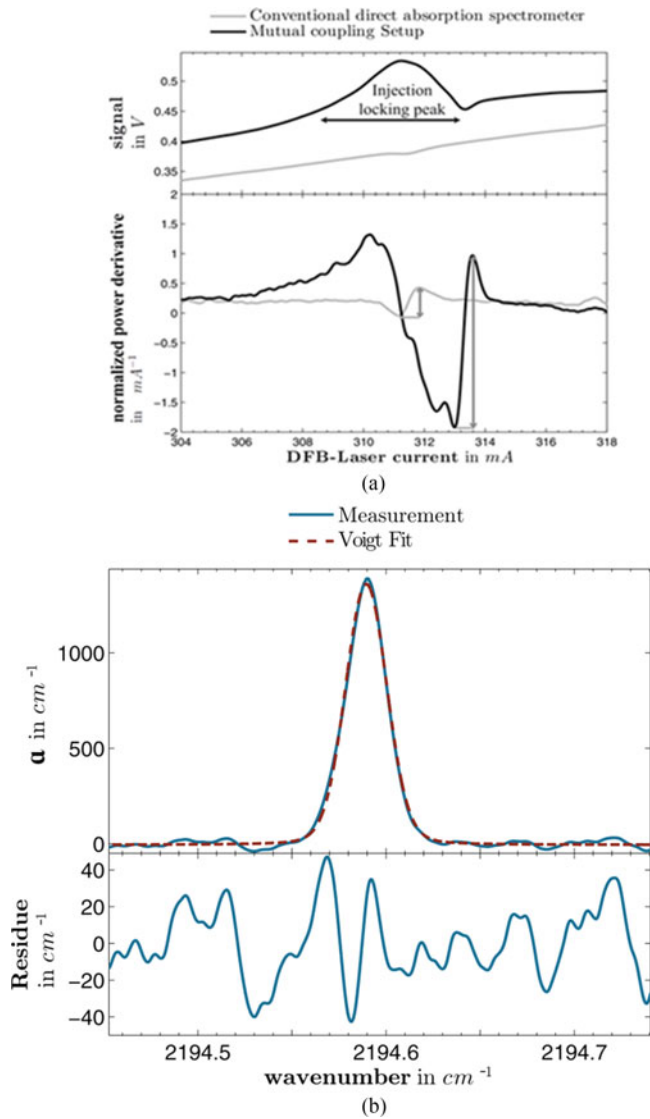


Fig. 8. (a) DFB-QCL power with and without mutual coupling setup (top) and its normalized derivative (bottom). (b) Absorption coefficient spectrum of 31 ppm of N₂O at a pressure of 280 hPa.

experiment we managed to decrease the FP laser threshold to 213 mA due to a better thermal conduction. We found that the point of larger sensitivity and thus higher enhancement is the point at the boundary of the locking bandwidth with the sharper transfer characteristic as predicted. This point corresponds to $I_{FP} = 201.5$ mA, the current value for which the boundary of the locking bandwidth coincides with the absorption dip. Fig. 9 also shows that the increase in sensitivity is realized for a wide range of gas concentration values from 15 to 626 ppm.

Finally, we measured the sensitivity enhancement factor as a function of the injection strength varied with the use of the NDF. We found in all cases that the maximum enhancement factor was recorded at the injection maximum strength which obviously enhances the power of the system and also changes the slope of the transition to the locking state, thus benefiting the sensing process.

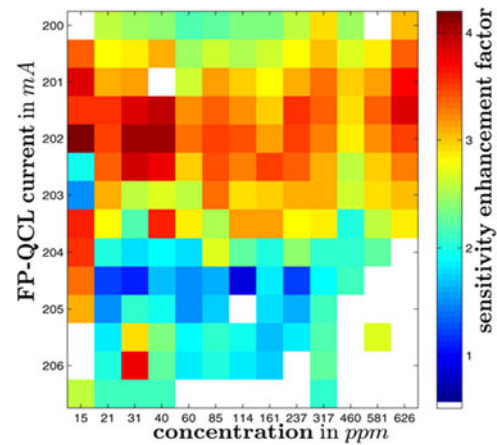


Fig. 9. Sensitivity enhancement factor in the plane of the FP-QCL current (here in this case: due to a better thermal conduction the FP-QCL threshold decreased to 213 mA) and the N₂O gas concentration in ppm. DFB-QCL was ramped from 2194.2 cm⁻¹ to 2195.3 cm⁻¹ with a frequency of 137 Hz, gas pressure amounted to (200 ± 20) hPa.

V. CONCLUSION

We presented a novel gas sensing scheme relying on a pair of mutually coupled QCL sources. The dynamical behavior of the system has been analyzed both experimentally and numerically. We highlighted its sensitivity to injection power, bias currents of the lasers and their spectral detuning. The analysis showed that this pair of lasers can operate as a high sensitivity gas sensor provided that one of the two lasers is biased around threshold. In this regime, the pair of lasers operates as an injection locked laser system with enhanced sensitivity against the optical injected power. Based on this principle, we performed gas sensing experiments, by using a sensing cell positioned in the optical path between the two lasers. When the laser system is operated in the transition regime from the non-locking to locking state, a six times enhanced sensitivity for N₂O absorption is proven in comparison to a typical absorption spectrometer consisting of a QCL source, a sensing cell and a typical MCT detector. We also carried out measurements for a wide range of gas concentration values and verified the enhanced sensitivity provided by the new sensor. The system shows to be very stable and in addition can be operated without the use of the MCT detector if one utilizes one of the two lasers as the detector by simply monitoring its voltage [22], [23]. With this perspective, the laser system has the potential of monolithic integration which would stimulate a wide range of applications. In order to further exploit the enhanced sensitivity of the proposed scheme, we intend to develop models which will allow the estimation of the concentration of target species solely based on the measurements taken from the specific system in the near future. Apart from its sensing benefits, the laser system is fundamentally interesting from the viewpoint of nonlinear dynamics and THz generation, subjects that we intend to explore in the near future.

ACKNOWLEDGMENT

The authors would like to acknowledge M. Carras from III-V Lab (now with mirSense) for providing us the FP laser.

REFERENCES

- [1] F. K. Tittel, D. Richter, and A. Fried, "Mid-infrared laser applications in spectroscopy," *Solid-State Mid-Infrared Laser Sources*. Berlin, Germany: Springer, 2003, pp. 458–529.
 - [2] F. Capasso, "High-performance midinfrared quantum cascade lasers," *Opt. Eng.*, vol. 49, no. 11, Nov. 2010, Art. no. 111102.
 - [3] R. F. Curl *et al.*, "Quantum cascade lasers in chemical physics," *Chem. Phys. Lett.*, vol. 487, no. 1, pp. 1–18, Jan. 2010.
 - [4] J. H. van Helden, R. Peverall, and G. A. D. Ritchie, "Chapter 2: Cavity enhanced techniques using continuous wave lasers," in *Cavity Ring-down Spectroscopy: Techniques and Applications*, G. Berden and R. Engeln, Eds., Chichester, U.K.: Wiley, 2009, pp. 27–56.
 - [5] D. D. Nelson, J. H. Shorter, J. B. McManus, and M. S. Zahniser, "Subpart-per-billion detection of nitric oxide in air using a thermoelectrically cooled mid-infrared quantum cascade laser spectrometer," *Appl. Phys. B*, vol. 75 pp. 343–350, Sep. 2002.
 - [6] B. W. M. Moeskops, S. M. Cristescu, and F. J. M. Harren "Subpart-per-billion monitoring of nitric oxide by use of wavelength modulation spectroscopy in combination with a thermoelectrically cooled, continuous-wave quantum cascade laser," *Opt. Lett.*, vol. 31, pp. 823–825, Mar. 2006.
 - [7] Y. Ma, R. Lewicki, M. Razeghi, and F. K. Tittel, "QEPAS based ppb-level detection of CO and N₂O using a high power CW DFB-QCL," *Opt. Express*, vol. 21, pp. 1008–1019, Jan. 2013.
 - [8] W. Brunner and H. Paul, "On the theory of selective intracavity absorption," *Opt. Commun.*, vol. 12, pp. 252–255, Nov. 1974.
 - [9] R. Provencal *et al.*, "Cavity-enhanced quantum-cascade laser-based instrument for carbon monoxide measurements," *Appl. Opt.*, vol. 44, pp. 6712–6717, Nov. 2005.
 - [10] G. N. Rao and A. Karpf, "High sensitivity detection of NO₂ employing cavity ringdown spectroscopy and an external cavity continuously tunable quantum cascade laser," *Appl. Opt.*, vol. 49, no. 26, pp. 4906–4914, Sep. 2010.
 - [11] K. M. Manfred, G. A. Ritchie, N. Lang, J. Röpcke, and J. H. van Helden, "Optical feedback cavity-enhanced absorption spectroscopy with a 3.24 μm interband cascade laser," *Appl. Phys. Lett.*, vol. 106, no. 22, Jun. 2015, Art. no. 21106.
 - [12] H. Erzgraeber *et al.*, "Mutually delay-coupled semiconductor lasers: Mode bifurcation scenarios," *Opt. Commun.*, vol. 255, no. 4–6, pp. 286–296, Nov. 2005.
 - [13] H. Simos, A. Bogris, D. Syvridis, and W. Elsaßer, "Intensity noise properties of mid-infrared injection locked quantum cascade lasers: I. modeling," *IEEE J. Quantum Electron.*, vol. 50, no. 2, pp. 98–105, Feb. 2014.
 - [14] T. Gensty and W. Elsaßer, "Semiclassical model for the relative intensity noise of intersubband quantum cascade lasers," *Opt. Comm.*, vol. 256, pp. 171–183, 2005.
 - [15] C. Juretzka *et al.*, "Intensity noise properties of midinfrared injection locked quantum cascade lasers: II. experiments," *IEEE J. Quantum Electron.*, vol. 51, no. 1, pp. 1–8, Jan. 2015.
 - [16] M. C. Soriano, J. García-Ojalvo, C. R. Mirasso, and I. Fischer, "Complex photonics: Dynamics and applications of delay-coupled semiconductor lasers," *Rev. Modern Phys.*, vol. 85, no. 1, pp. 421–470, Mar. 2013.
 - [17] C. Wang, F. Grillot, V. Kovanis, and J. Even, "Rate equation analysis of injection-locked quantum cascade lasers," *J. Appl. Phys.*, vol. 113, no. 6, pp. 063104-1–063104-6, Feb. 2013.
 - [18] G. Friart, G. Van der Sande, G. Verschaffelt, and T. Erneux, "Analytical stability boundaries for quantum cascade lasers subject to optical feedback," *Phys. Rev. E*, vol. 93, no. 5, May 2016, Art. no. 052201.
 - [19] K. S. Yong, M. K. Haldar, and J. F. Webb, "Theory of reduction of residual amplitude modulation in mid-infrared wavelength modulation spectroscopy by injection locking of quantum cascade lasers," *IEEE J. Sel. Topics Quantum Electron.*, vol. 21, no. 6, pp. 115–24, Nov. 2015.
 - [20] F. P. Mezzapesa *et al.*, "Intrinsic stability of quantum cascade lasers against optical feedback," *Opt. Express*, vol. 21, pp. 13748–13757, 2013.
 - [21] J. Ohtsubo, "Semiconductor Lasers: Stability, Instability and Chaos," New York, NY, USA: Springer, 2012.
 - [22] P. Dean *et al.*, "Terahertz imaging through self-mixing in a quantum cascade laser," *Opt. Lett.*, vol. 36, no. 13, pp. 2587–9, Jul. 2011.
 - [23] F. Michel, C. Juretzka, M. Carras, and W. Elsaßer, "30% improvement in absorption spectroscopy detectivity achieved by the detuned loading of a quantum cascade laser," *Opt. Lett.*, vol. 39, no. 21, pp. 6351–6354, Nov. 2014.
- Adonis Bogris** was born in Athens, Greece, on June 16, 1975. He received the B.S. degree in informatics, the M.Sc. degree in telecommunications, and the Ph.D. degree from the National and Kapodistrian University of Athens, Athens, in 1997, 1999, and 2005, respectively. His doctoral thesis was on all-optical processing by means of fiber-based devices. From 2000 he serves as a Researcher and External Collaborator at the Optical Communications Laboratory, National and Kapodistrian University of Athens, participating in local and European projects. He is currently an Associate Professor at the Department of Informatics of the Technological Educational Institute of Athens, Greece. He has authored or co-authored more than 100 articles published in international scientific journals and conference proceedings. His current research interests include high-speed all-optical transmission systems and networks, nonlinear effects in optical fibers, all-optical signal processing and all-optical networking, nonlinear effects in lasers and photonic waveguides, mid-infrared photonic devices, and cryptography at the physical layer. He serves as a reviewer for the journals of the IEEE.
- Andreas Herdt** was born in Wetzlar, Germany, on June 19, 1991. He received the B.Sc. degree in physics from the Technical University of Darmstadt in 2014. He is currently working with the group of Prof. Elsaßer (Technical University of Darmstadt) as a Master Student. He is Member of the German Physical Society.
- Dimitris Syvridis** received the B.Sc. degree in physics, the M.Sc. degree in telecommunications, and the Ph.D. degree in physics in 1982, 1984, and 1988, respectively. He was a Researcher with the Electronics Laboratory, National and Kapodistrian University of Athens, Athens, Greece, from 1988 to 1990. From 1990 to 1993, he was a Researcher with the Institute of Quantum Electronics, Swiss Federal Institute of Technology (ETH Zurich), Zurich, Switzerland. From 1993 to 1997, he was a Senior Researcher with the Department of Informatics, National and Kapodistrian University of Athens, where he is currently a Full Professor. He has participated in many European research projects on optical communications. He has authored or co-authored more than 200 papers in scientific journals and conference proceedings. His current research interests include optical communications and networks, photonic devices, and related subsystems, as well as photonic integration.
- Dr. Syvridis is a reviewer for journals of the IEEE.
- Wolfgang Elsaßer** (M'94–SM'98) was born in 1954 in Pforzheim, Germany. He received the Diploma degree in physics from the Technical University in Karlsruhe in 1980 and the Ph.D. degree in Physics from the University Stuttgart, Germany in 1984.
- From 1981 to 1985 he was with the Max-Planck-Institute for Solid State Research in Stuttgart, Germany. From 1985 to 1995 he was with the Philipps-University Marburg, Germany. In 1991 he was with the Habilitation in Experimental Physics at the Philipps-University Marburg. From 1995 he has been a Full Professor in the Institute of Applied Physics at the Technical University in Darmstadt (Technische Universität Darmstadt), Germany. In 1992 he took sabbatical at the Ecole Nationale Supérieure des Télécommunications, Paris, France. In 1990, 1996, 1999, 2000, and 2003 he had research stays at the Trinity College Dublin, Ireland, in 2003 at Fraunhofer Institut für Physikalische Meßtechnik Freiburg and Università di Firenze and LENS Firenze, and in 2007 at Politecnico di Torino and Università di Pavia. He was awarded with the Otto-Hahn-Medal (1985), the Werner-von-Siemens-Medal (1985), the Rudolf-Kaiser Prize (1991), the IEE J. J. Thomson Premium (1995), the 1st Hassia Cooperation Award of the Technology Foundation Hassia (jointly with Sacher Lasertechnik Marburg) in 2004, and in 2011 with the Award of the Darmstaedter Technology Transfer Foundation. He is a Member of the German Physical Society (DPG).